STUDY OF VARIOUS RE-ENTRY VEHICLE CONFIGURATIONS FOR FUTURE INTERPLANETARY MISSIONS

M. I. Afzal; M.H. Gräßlin; H.-P. Röser
Institute of Space Systems, University of Stuttgart, Pfaffenwaldring 31, D-70569 Stuttgart, Germany

ABSTRACT

Future long-term plans for the robotic or human exploration of solar system bodies (e.g. AURORA program in Europe) demand new and innovative concepts for the design of vehicles which can enter a planetary atmosphere and land on its surface safely. Vehicle approaching a planet at hyperbolic speed passes through its atmosphere with very high thermal and mechanical loads. Vehicle and mission design process requires a thorough investigation of this flight phase and its sensitivity to environmental influences and uncertainties as well as vehicle properties. The main emphasis of this report is the Earth capture and re-entry phase of human interplanetary return mission. The report assesses the performance of 3 different configurations of re-entry vehicles for stagnation point heat fluxes, total heat loads and g-loads. Apollo like capsule with an L/D ratio of about 0.3, flattened bi-conic with an L/D ratio of about 0.7 and winged vehicle with an L/D ratio of about 2.2 are categorised as low, medium and high lifting vehicles.

1 INTRODUCTION

Analysis of reentry trajectory is currently a main topic in space flight mechanics research. The interest is partly due to the large improvements in computing and modeling techniques that are a basic instrument for such kind of analysis. Vehicle approaching a planet at hyperbolic speed possesses a large amount of kinetic energy and potential energy. This energy is converted into heat while the vehicle passes through planetary atmosphere with very high thermal and mechanical loads. Trajectory analysis of such a vehicle involves both dynamic and thermal requirements, and due to complex interacting phenomena, usually requires a numerical analysis.

An important problem associated with entries at super-orbital speeds is that of entry corridor required in order to accomplish a desired entry maneuver, such as entering without encountering excessive deceleration or heating loads. In contradiction to sub-orbital flights the tolerances at entry condition are relatively narrow, since an undershoot or a steep entrance my cause destruction of vehicle during entry, and an overshoot may result in a skip-out or a homeless exit into space.

Analysis of reentry trajectories allows an attempt of systematic classification of spacecraft types and reentry methods. As far as spacecraft is concerned aspects of lift to drag ratio and ballistic coefficients lead to the difference between ballistic, semi-ballistic and lifting trajectories.

The main emphasis of this report is the Earth capture and re-entry phase of human interplanetary return mission. The early lunar return missions were accomplished with a so-called ‘capsule’ shaped vehicle. There are however significant disadvantages of capsule design, especially the load factor of more than 7 times of Earth gravitation, which exceeds 4.0 g’s limit of NASA’s safety standards for astronauts.

The report assesses the performance of 3 different configurations of re-entry vehicles for stagnation point heat fluxes, total heat loads and g-loads. Apollo like capsule with an L/D ratio of about 0.3, flattened bi-conic with an L/D ratio of about 0.7 and winged vehicle with an L/D ratio of about 2.2 are categorised as low, medium and high lifting vehicles. Flattened bi-conic and winged vehicles use aerodynamic lift to remain at certain constant altitude to get rid of excessive kinetic energy before descending to the earth surface, whereas Apollo like capsule, due to its low lift to drag ratio, can stay at constant altitude for only a short period and descends faster through the earth atmosphere. A comparative re-entry performance analysis is performed among three configurations for four parameters – stagnation point heat flux, integral heat load, peak deceleration (g-load).

Analysis of reentry trajectories involves both dynamic and thermal requirements, and due to complex interacting phenomena, usually requires a numerical analysis. A three degree of freedom trajectory simulation tool is used to simulate re-entry trajectories in a three dimensional space while treating the vehicle as a point mass. The simulation tool uses a non-linear programming (NLP) approach to find optimum trajectories for a predefined cost function (such as maximum heat flux, integral heat load, maximum deceleration load etc.) as a function of a finite number of control parameters with upper and lower bounds and subjected to equality and inequality constraints. Stagnation point heat flux, integral heat load, radiation heat flux and aerodynamic deceleration loads are calculated during trajectory simulation to study the influence of vehicle and atmospheric properties on these important parameters.

2 REFERENCE MISSION

The reference mission for this analysis is a lunar return mission with an orbital inclination of return trajectory of 28.5° with respect to earth equator. For this analysis a Kepler orbit is considered with assumed apogee of 385,000 km, which is the average distance of Moon from centre of Earth. Perigee of the orbit is selected in such a way to get an entry angle of -6.5°, -4.9°, and -4.0° for Apollo-like capsule, flattened bi-conic, and high lifting vehicles respectively at Earth atmospheric interface of 120

km above Earth surface. The velocity at this interface is approximated to 11.0 km/sec for all three entry conditions (Interplanetary return missions usually return at velocities ranging between 11 to 12 km/sec).

3 Re-entry Strategy

Two kinds of re-entry approaches are considered for re-entry trajectory simulations; direct *re-entry* for Apollo-8 re-entry module because of its low lift to drag ratio and re-entry with constant altitude phase for lifting vehicles, which utilize their lift to maintain a constant altitude in order to decelerate at low heat fluxes. Fig. 1 shows both candidate trajectories.

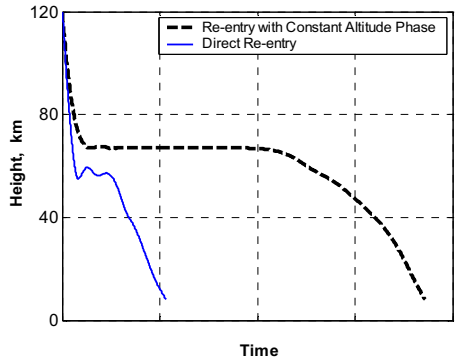

Figure 1: Candidate re-entry trajectories

3.1 Direct Re-entry

In general, spacecrafts returning to the Earth from an interplanetary mission adopt a direct re-entry strategy. The direct entry trajectory offers the advantage of a “no-miss” scenario where starts at steep entry angle, quickly dissipating excessive kinetic energy, which results in a very high level of deceleration and heat loads. The main parameter that drives a trajectory to “direct” is the perigee of the lunar return orbit. In many unmanned re-entry missions, a ballistic entry method is adopted, where only drag force slows down the vehicle. A purely ballistic entry, in which deceleration levels during re-entry are extremely high, is not survivable by human crew. A semi-ballistic approach is useful in this case, where appropriate control method is used to generate lift in order to reduce deceleration and heat loads.

3.2 Re-entry with Constant Altitude Phase

Exploiting lift forces during interplanetary re-entry is being considered by researchers around the world to get more control over the trajectory and guide the spacecraft more precisely to a landing site. Vehicles concepts other than a blunt body, like winged, bi-conic, inflatable ballute design etc. were presented from time to time at various platforms.

The orbit of the return trajectory is so designed that the vehicle intercepts the outer atmosphere and then exploits vehicle lift to fly at constant altitude and dissipating excess energy using aerodynamic drag.

4 VEHICLE CONFIGURATIONS

4.1 Apollo-like Capsule

Apollo-8 (Fig. 2) re-entry module returned from a manned lunar mission on Dec. 27, 1968,[1] is selected as one of the three candidate vehicles for comparative analysis. Because of its low lift to drag ratio of 0.3, this vehicle enters directly into the Earth atmosphere experiencing high heat and deceleration loads. Aerodynamic properties (Fig. 3) of Apollo-8 re-entry module are investigated based on equations derived by *Sforza,*[2] and CFD investigations of *Padila* and *Boyd*.[3] On this basis initially an average value of 1.4 for drag coefficient and 0.3 for L/D ratio is taken for a fixed angle of attack of 20° and for 12.02 m^2 of reference area.

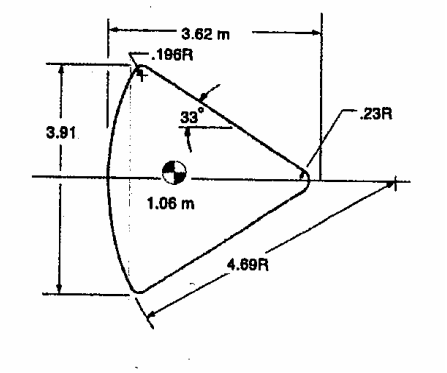

Figure 2: Apollo-8 re-entry module[1]

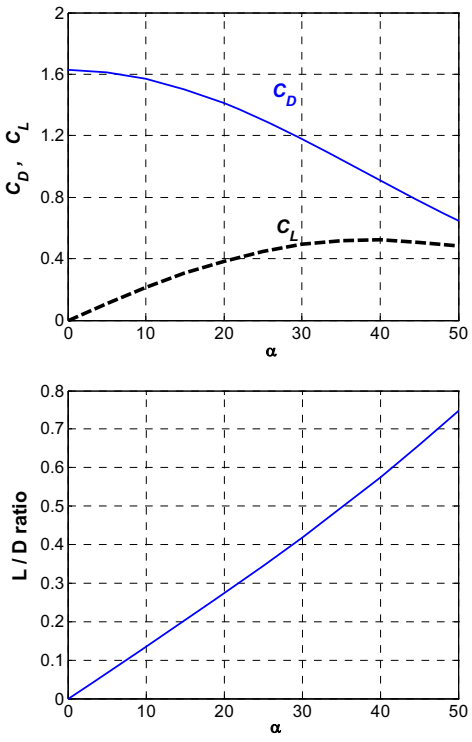

Figure 3: Apollo-8 aerodynamic coefficients

Re-entry trajectory of Apollo-8 module is then simulated for entry velocity of 11 km/s, entry angle of -6.5° and entry mass of 5700kg, with bank angle modulation to use the lift in order to minimize stagnation point heat flux as well as to reach target point. Bank angle during the initial descent phase is so modulated that stagnation point heat flux is minimized till the vehicle starts ascending again. Thereafter bank angle is modulated to follow actual trajectory curve of Apollo-8 re-entry module as given in post flight mission reports.[4,5,6] Fig. 4 below compares altitude and flight path angle histories of simulation results and actual trajectories.

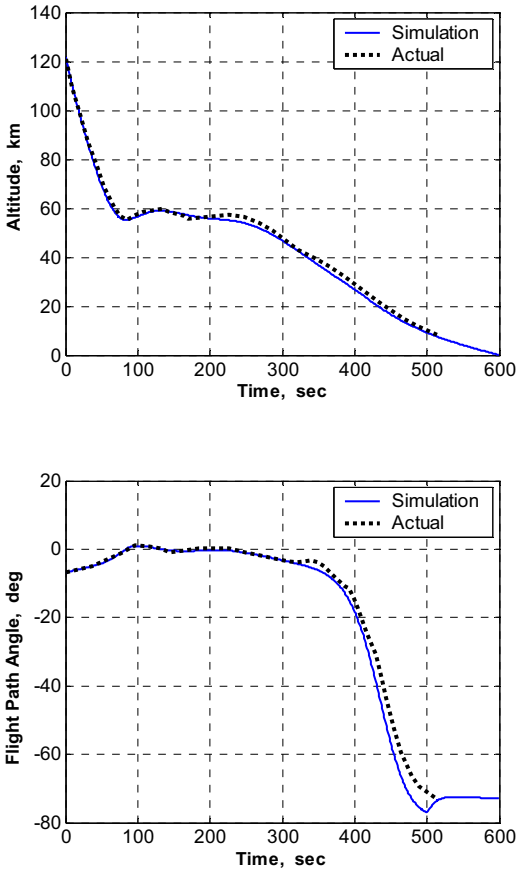

Figure 4: Apollo-8 re-entry trajectory simulation

4.2 High Lifting Vehicle

Exploiting lift forces for manned interplanetary re-entry missions has been an interesting research topic, because of high deceleration loads of more than 7 g's during re-entry of early Apollo missions. Different re-entry strategies like aero-capture, aero-breaking and different vehicle concepts were studied from time to time by different space agencies and institutes. A concept of winged vehicle with high aerodynamic efficiency (Fig. 5) entering Earth atmosphere at hyperbolic velocities was proposed by Monti, et al.[7] This vehicle is considered here as a candidate for comparative analysis.

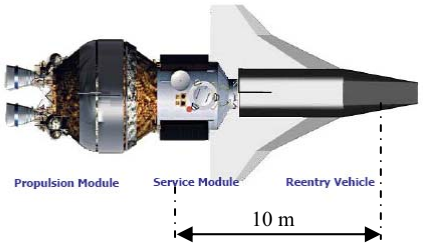

Figure 5: High lifting vehicle[7]

Newtonian flow approximation is considered to calculate drag and lift forces, because it is a simple and attractive method for developing simple relationships to predict the aerodynamic properties of bodies at hypersonic speeds. Following relations given by Anderson[8] for drag and lift coefficient are considered.

$$C_D = 2\sin^3\alpha$$
$$C_L = 2\sin^2\alpha\cos\alpha$$

Reference area for aerodynamic calculations is the planform area of the vehicle which is about 50m^2.

Re-entry approach with constant altitude phase is used with a trajectory that has a higher perigee of lunar return orbit only intercepts the outer atmosphere. The trajectory from space to ground is divided into three phases:

1. *Approach phase*; which starts with the entry of vehicle into the Earth atmosphere at 120 km above mean sea level, at entry velocity of 11.0 km/s, entry angle of -4.0° and entry mass of 5000kg. Vehicle at super-orbital speed generates enough centrifugal force to skip again out of upper atmosphere. To balance this centrifugal force vehicle enters at an initial bank angle of 180° at atmospheric interface (i.e. upside down) in order to have a component of lift in a direction to Earth centre. In this way vehicle is able to be captured by earth atmosphere.
2. *Constant altitude phase*; with control law the lift is controlled by angle of attack variation and also bank angle modulation, in order to keep the altitude constant. Vehicle's drag slowly decelerates the vehicle during this phase and hence required angle of attack also reduces to maintain the altitude. Practically the vehicle is required to be insulated mostly on one side i.e. on the side of stagnation point. In this regards a control law find values of angle of attack not lower than a certain value, e.g. 20°. Bank angle is modulated to get the desired lift in vertical plane when the angle of attack requirement is lower than 20°. Bank angle is gradually reduced from 180° to 90° (or 270°) where speed become equal to instantaneous orbital speed and then further change to 0° as the speed also gradually reduces.
3. *Descend phase*; starts when the speed of the vehicle is reduced during constant altitude phase to such a level that it can safely bring down to the Earth surface. Bank angle is again modulated during this phase to reach desired landing site.

Trajectory of high lift vehicle is simulated for above mentioned entry conditions and entry strategy and show in figures below (Fig. 6). As seen in bank angle profile that vehicle enters upside down until a point where angle of attack is reduced to a lower limit of 20°. There after angle of attack does not reduce further and bank angle is modulated to compensate for lift requirement. Once the excess lunar-return kinetic energy has been dissipated the vehicle gradually rolls upright and proceeds further with upward lift vector to maintain the altitude and reduce further energy.

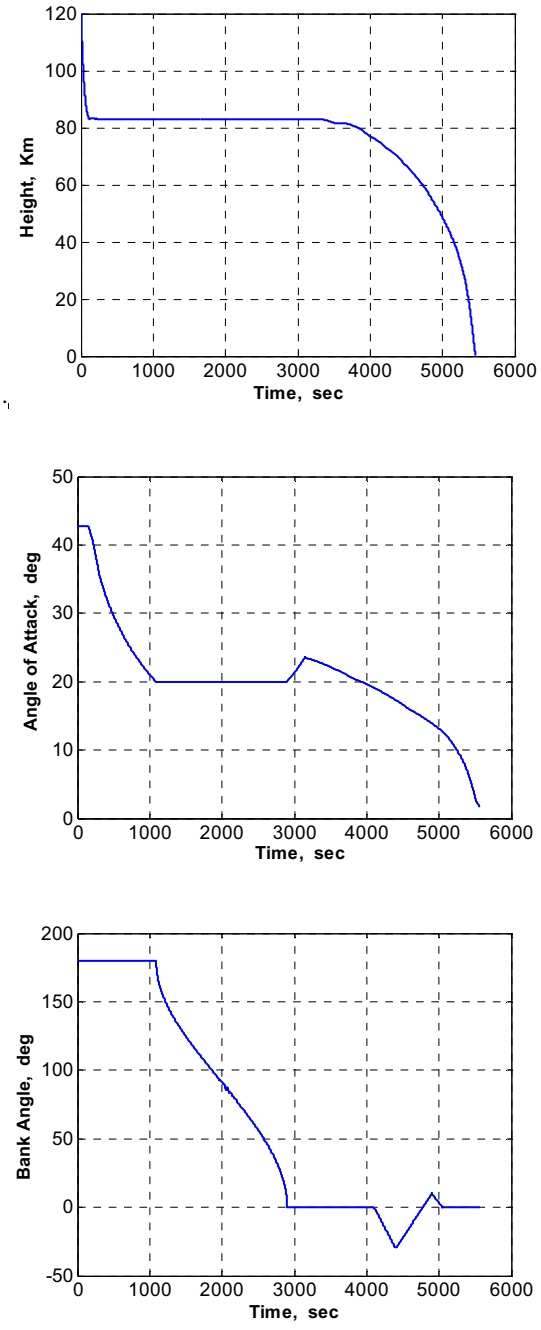

Figure 6: High lifting vehicle trajectory simulation

4.3 Flattened Bi-conic Vehicle

Apollo like capsule having an advantage of the simplest design enters at high deceleration levels. This is exactly opposite for high lifting vehicle which despite experiences very low deceleration load is very complex in design. Flattened bi-conic vehicle (Fig. 7), presented by Whitmore, et al.[9] lies in between the two, is relatively simple in design and it is selected as third candidate vehicle for comparative analysis here but scaled down for a total mass of 5000kg. Aerodynamics coefficients for a reference area of 6.9 m^2 as shown in figure below (Fig. 8) are assumed to be same as trimmed longitudinal aerodynamic data of Whitmore.[9]

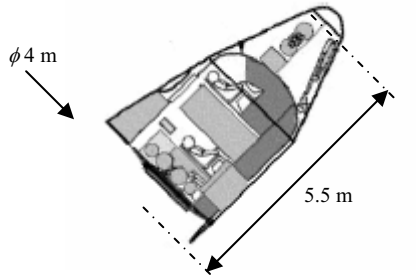

Figure 7: Flattened bi-conic vehicle[9]

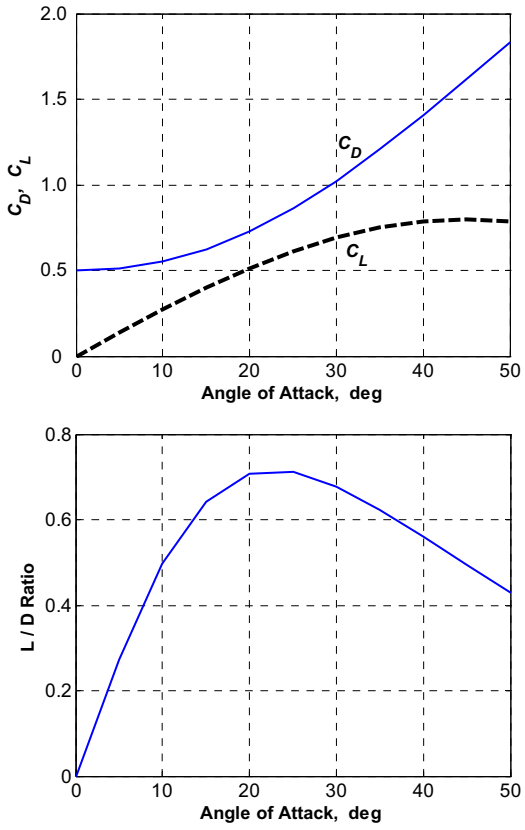

Figure 8: Flattened bi-conic aerodynamic coefficients

Like high lifting vehicle, re-entry approach with constant altitude phase is used for flattened bi-conic vehicle, with a trajectory that has a perigee of lunar return orbit lower than the case of high lifting vehicle but higher than Apollo-8 re-entry module. Following the same strategy for angle of attack control and bank angle modulation, the re-entry trajectory of flattened bi-conic vehicle is simulated and presented below (Fig. 9).

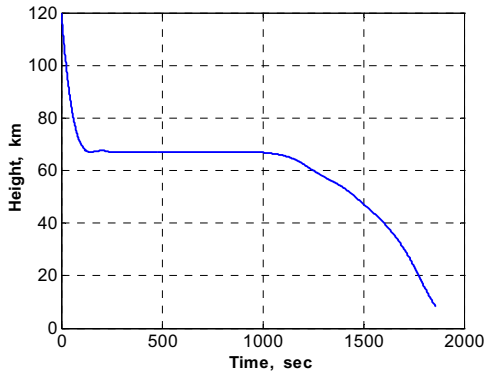

Figure 9: Flattened bi-conic trajectory simulation

Another re-entry approach for flattened bi-conic vehicle is under consideration to reduce the total heat load. In this approach vehicle is allowed to skip out of atmosphere to a predefined altitude and re-entering again in the atmosphere. It is assumed that the heat absorbed by the vehicle during first entry is rejected during the skip phase thereby reducing the total heat load.

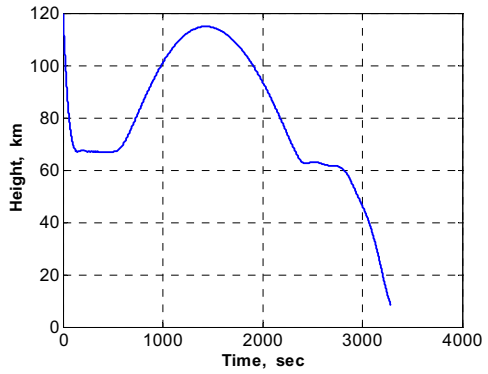

Figure 10: Flattened bi-conic trajectory simulation

5 ASSESSMENT OF CONFIGURATIONS

5.1 Vehicle Design

This section presents a comparison of the geometry of vehicles under consideration. Vehicle design of Apollo capsule, high lifting and flattened bi-conic vehicles are already shown in figures 2, 5 and 7 respectively. Table 1 is presented below to show important physical parameters of these vehicles. Reference area of Apollo capsule, high lifting and flattened bi-conic vehicles are based on maximum cross-section area, wing planform area and flattened area respectively. High lift vehicle is found to be relatively light in terms of ballistic coefficient, because of its large reference area.

Volumetric efficiency is a critical packaging parameter and is defined as volume of the vehicle divided by the cube of the largest external dimension. In general the blunter the vehicle, the higher is the volumetric efficiency. A sphere as an example has theoretically the highest possible volumetric efficiency of about 0.5236. In this sense Apollo capsule is having the highest and high lifting vehicle is having the lowest volumetric efficiency among the candidate vehicles under consideration. The volumes are calculated by approximating various geometrical segments of the vehicles for the volumes of spherical caps, cylinders, cones and conical frustums. The volume of wings is not considered here.

Table 1: Comparison of Vehicles Geometric Design

	Capsule	High-lift	Bi-conic
Mass (*kg*)	5706	5000	5000
Length (m)	3.6	10.0	5.5
Diameter (m) (wing-span)	3.9	9.0	4.0
Nose Radius (m)	4.69	0.10	0.75
Ref. Area (m^2)	12.02	50.0	6.90
Ballistic Coefficient (kg/m^2)	340	63	400
Approx. Volume (m^3)	14	30	25
Volumetric Eff. (V / L^3)	0.23	0.03	0.15

5.2 Maximum Heat Rate

Vehicle approaching a planet at hyperbolic speed possesses a large amount of kinetic energy and potential energy. When it enters the atmosphere, a shock wave is formed ahead of its nose, heating the atmosphere in this region to a very high temperature. The aero-thermal loads on the surface of vehicle are estimated at the stagnation point, applying simplified empirical relations. The convective heat transfer rate at stagnation points is calculated by applying a simple and well known method given by Anderson.[10]

$$q_c = 1.83\times10^{-8} V_\infty^3 \sqrt{\frac{\rho_\infty}{R}}$$

Where ρ_∞ and V_∞ are the free air density and speed and R is the nose radius.

Intense radiative heat transfer from high temperature shock layer to the surface of super-orbital re-entry vehicle is also an important engineering consideration in the design of thermal protection system. In orbital and sub-orbital re-entry vehicles the radiation heat transfer is negligibly small. A simplified method to calculate radiative heat transfer rate given by Tauber and Sutton[11] is adopted here.

$$q_r = 4.736\times10^4 R^a \rho_\infty^b f(V_\infty)$$

Where $f(V_\infty)$ are tabulated values (see [11]) and exponent *a* and *b* are as follows.

$$a = 1.072 \times 10^6 V_\infty^{-1.88} \rho_\infty^{-0.325}$$

$$b = 1.22$$

Anderson[12] compared radiative and convective heat transfer rates of a re-entry vehicle with nose radius of 4.57m at an altitude of about 61 km as a function of velocity, which is shown below (Fig. 11). The limitation of Tauber's model that it does not calculates radiation heat flux for vehicle velocity lower than 9 km/s is clear in this figure, where it can be seen that near a velocity of 10 km/s, the radiation heat flux decreases rapidly with velocity.

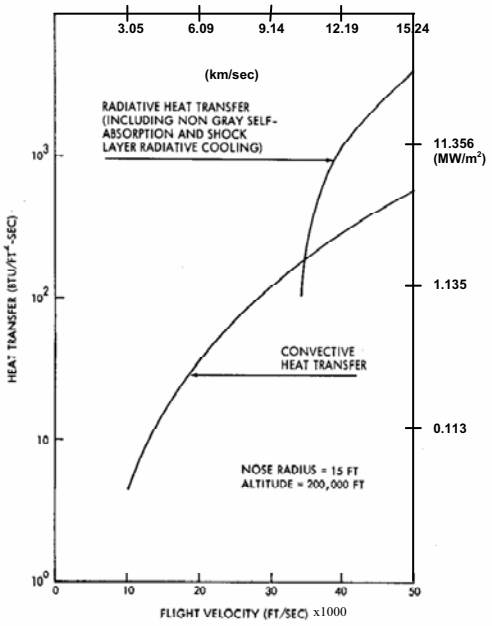

Figure 11: Comparison of radiative and convective stagnation point heat transfer[12]

A comparison of stagnation point heat transfer rates for both convection and radiation is shown in figures below (Fig. 12 - 14) based on above mentioned methods. The convective heat transfer at stagnation point in the adopted method is directly proportional to the square root of atmospheric density and inversely proportional to the square root of nose radius. High-lift vehicle maintain a higher constant altitude, where the density is relatively low, but due very small wing tip radius it is subjected to a higher stagnation point convective heat flux as compare to Apollo capsule (Fig. 12). Flattened bi-conic vehicle, because of its small nose radius and lower constant altitude flight experiences the highest convective heat rate at stagnation point among three vehicles.

The radiative heat transfer at stagnation point in the adopted method is proportional to both atmospheric density and nose radius of the vehicle. This is the reason that high lift vehicle having very small wing tip radius and high constant altitude flight experiences very low stagnation point radiative heat flux. Apollo capsule, in this manner experiences the highest stagnation point radiative heat flux among three vehicles. Total heat flux is also presented in a figure below (Fig. 14). Peak radiation heat flux is found to be 39%, 13%, and 1% of the peak total heat flux for Apollo, bi-conic and high-lift vehicles respectively.

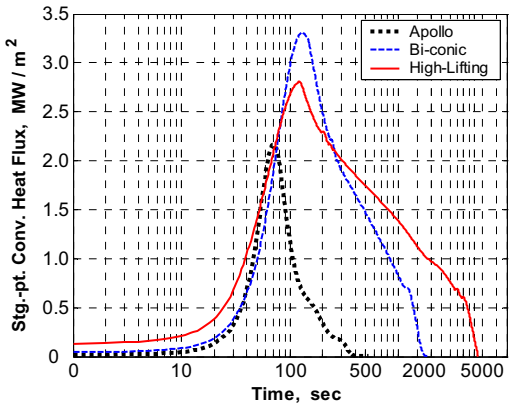

Figure 12: Comparison of convective stagnation point heat transfer

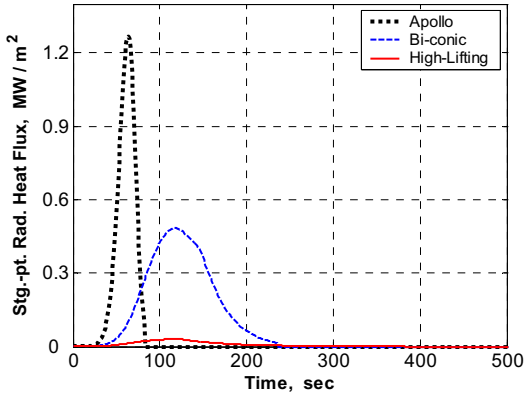

Figure 13: Comparison of radiative stagnation point heat transfer

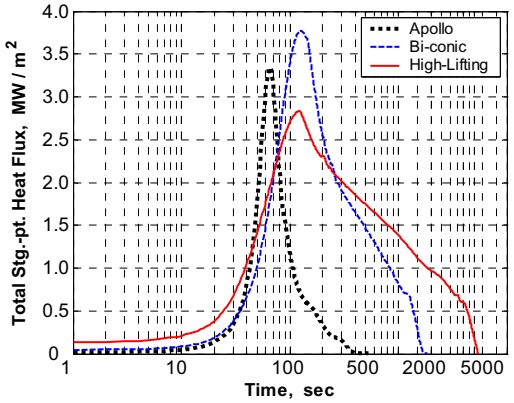

Figure 14: Comparison of total stagnation point heat transfer

5.3 Integral Heat Load

Integral or total heat derives thickness of the thermal protection system. High-lift vehicle although experiences lowest stagnation point heat flux among three vehicles, due to its long constant altitude flight, total heat absorbed by the vehicle is much greater. The following table compares maximum stagnation point heat rate, integral

heat load and total flight time for nominal entry and environmental conditions.

Table 2: Comparison of Heat Loads

	Capsule	Bi-conic	High-lift
Entry Velocity (*km/s*)	11	11	11
Entry Angle	-6.5°	-4.9°	-4.0°
Max Heat Rate (MW/m^2)	3.34	3.77	2. 84
Integral Heat Load (MJ/m^2)	225	1906	4908
Flight Time (*sec*)	532	1858	5456

Mass and thickness of thermal protection system is not calculated here, but a heavy amount of thermal protection system would be required for high-lift vehicle to prevent it from heat absorption, which already has a very low volumetric efficiency. This could lead the vehicle to be infeasible for such a mission.

5.4 Deceleration

Deceleration load during re-entry is also an important parameter, especially for safety and comfort of the crew in case of manned mission. Man-Systems Integration Standards[13] defined by NASA for physically de-conditioned astronauts are considered here, which states that: 1) peak deceleration level during re-entry can not exceed 4.0 g's for a de-conditioned astronaut sitting upright position, 2) peak deceleration level during re-entry can not exceed 4.0 g's for a de-conditioned astronaut sitting reclined position. A de-conditioned astronaut is defined as a person who has been exposed to zero-g or micro-gravity conditions for a period of two weeks or more.

Apollo capsule enters directly into the atmosphere with steep entry angle, decelerates at high loading of more than 7 g's (Fig. 15), which is more than the current safety standards for astronauts. Lift force in case of flattened bi-conic and high-lift vehicles is exploited to keep them flying at constant altitude where atmospheric density is lesser and thereby decelerating at much slower rate until they enter sub-orbital speed regime. Peak deceleration for flattened bi-conic and high-lift vehicles noted from re-entry trajectory simulations are 1.5 g's and 1.2 g's respectively. Figure below (Fig. 15) shows histories of deceleration rate for all three candidate vehicles.

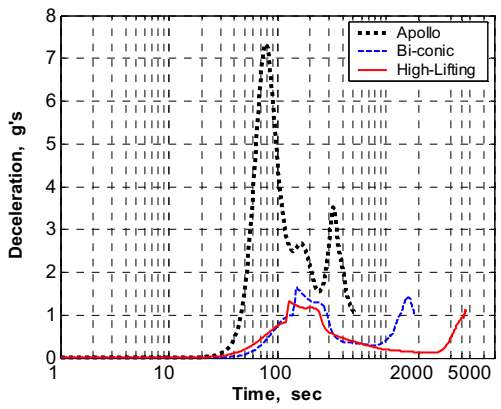

Figure 15: Comparison of deceleration load

5.5 Entry Corridor

Analysing entry corridor of Apollo capsule differs from other two vehicles because their different entry approaches. In case of Apollo capsule peak stagnation point heat flux and peak deceleration level are important and define the boundaries of entry corridor. Peak deceleration levels in case of other two vehicles are already on much lower side. Another important factor in this case that defines the boundary of entry corridor is the ability of vehicles to keep flying at pre-defined constant altitude without skipping again.

Entry corridor of Apollo capsule is shown below (Fig. 16). Both - peak stagnation point heat flux and peak deceleration level increase - with increase of either velocity or entry angle. Dashed line in figure shows a limit of 8.0 g's of deceleration load. On the right side of this line vehicle enters the earth atmosphere but with more than 8.0 g's of deceleration load.

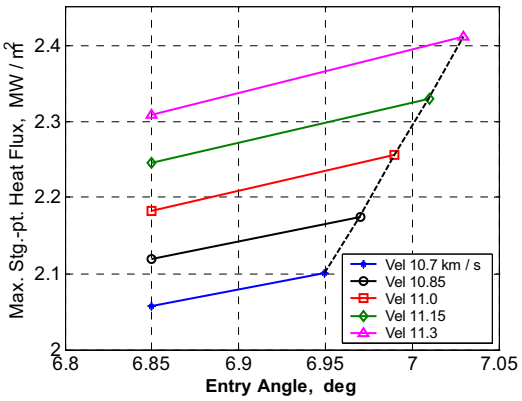

Figure 16: Entry corridor - Apollo capsule

Analysis of entry corridor of flattened bi-conic and high-lift vehicles is done and shown in parallel to each other in a figure below (Fig. 17). Any trajectory starting with entry conditions on the right side of shaded zone enters the Earth atmosphere with a peak stagnation point heat flux of 0.1 MW / m^2 additional to the nominal conditions. And any trajectory with entry conditions on the left side of shaded zone is not possible as the vehicle skip out again due to high centrifugal force. This also defines the controllability of vehicle.

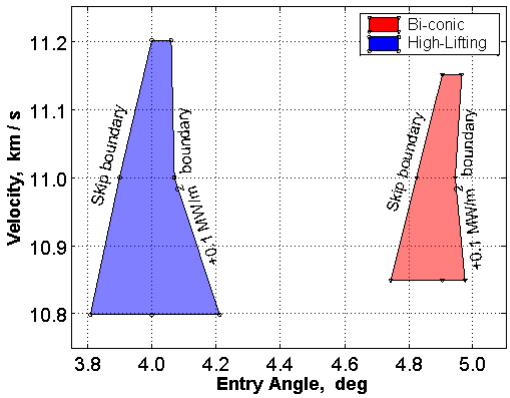

Figure 17: Entry corridor: flattened bi-conic and high-lift vehicles

6 CONCLUSION

Re-entry trajectories are simulated for three different configurations of re-entry vehicles returning Earth from a lunar mission. A comparison of vehicle geometric design is presented and an assessment of simulation results is done for stagnation point heat rate, integral heat load, deceleration load and entry corridor.

Apollo like capsule being the simplest design and having best volumetric efficiency, enters into the atmosphere with steep entry angle, following a direct entry strategy and decelerates at high loading of more than 7 g's which is more than the current safety standards for astronauts.[13] High deceleration load is the main disadvantage of this type of vehicle and this is the reason that alternate vehicle configurations are studied and compared here.

High-lift vehicle keeps a constant altitude where the atmospheric density is much less and therefore flying at much lower deceleration loads. Relatively sharp wing tips are subjected to high heat rate, for which ceramic material is proposed by *Monti*, et al.[7] Total heat input to the vehicle is almost 22 times the integral heat load of Apollo capsule. Already having low volumetric efficiency, a large amount of thermal protection would be required to protect the vehicle itself, and astronauts and instruments inside it.

Flattened bi-conic re-enters at lower deceleration load of around 2 g's but with higher stagnation point and higher total heat load, about 8 times the integral heat load of Apollo capsule. Ablative materials high heat rates as used in Apollo capsule can also be easily used here. Total heat input to the vehicle requires more thermal protection system to be applied, which would reduce the space required for the astronauts and instruments inside.

Flattened bi-conic vehicle found to be most suitable among three vehicles because; its design is not complex as high-lift vehicle, it does not experiences very high deceleration load like Apollo capsule, nor it experiences very high integral load like high-lift vehicle.

7 ACKNOWLEDGEMENT

This study is a part of doctoral research, being carried out at Institute of Space Systems, University of Stuttgart, in the field of interplanetary entry missions. The research work is funded by Higher Education Commission of Pakistan (HEC) in collaboration with Deutsch Akademischer Austausch Dienst e.V. (DAAD), Germany.

8 REFERENCES

[1]. Planetary Mission Entry Vehicles, Quick Reference Guide, Version 2.1; *NASA Ames Research Centre*.

[2]. *Pasquale M. Sforza*; EAS4710 Aerospace Design 2 – Space Access Vehicle Design, Department of Mechanical and Aerospace Engineering, University of Florida; *http://aemes.mae.ufl.edu/~sforza/EAS4710*

[3]. *Jose F. Padilla, Iain D. Boyd*; Assessment of Rarefied Hypersonic Aerodynamics Modelling and Wind Tunnel Data; *AIAA 2006-3390*

[4]. Apollo-8 Mission Report; *NASA, MSC-PA-R-69-1*; *Manned Spacecraft Centre, Houston, Texas, February 1969*.

[5]. Apollo-8 Mission Report - Trajectory Reconstruction and Post-flight Analysis; *NASA, MSC-PA-R-69-1 Supplement 1*; *Manned Spacecraft Centre, Houston, Texas, November 1969*.

[6]. Apollo-8 Mission Report – Guidance, Navigation and Control System Performance Analysis; *NASA, MSC-PA-R-69-1 Supplement 2*; *Manned Spacecraft Center, Housten, Texas, November 1969*

[7]. *R. Monti, R. Janovsky, M. De Stefano Fumo*; Exploiting Lift Force in Re-entries from Exploration Missions; *DGLR International Symposium 'To Moon and Beyond', Bremen, 2007*.

[8]. *Anderson, J. D.*; Hypersonic and High Temperature Gas Dynamics; *AIAA, 2006, Chapter 3, pp 59.*

[9]. *Stephan A. Whitmore, Daniel W. Banks, Benjamin M. Andersen, Patrick R. Jolley*; Direct-Entry, Aero-braking, and Lifting Aero-capture for Human-Rated Lunar Return Vehicles; *AIAA-2006-1033*.

[10]. *Anderson, J. D.*; Hypersonic and High Temperature Gas Dynamics; *AIAA, 2006, Chapter 6, pp 349.*

[11]. *M. E. Tauber, K. Sutton*; Stagnation-Point Heating Relations for Earth and Mars Entries; *Journal of Spacecraft, Vol. 28, No. 1, Jan-Feb 1991*

[12]. *Anderson, J. D.*; An Engineering Survey of Radiating Shock Layers; *AIAA Journal, Vol. 7, No. 3, September 1969.*

[13]. Man-Systems Integration Standards - NASA Technical Standards Program; *NASA-STD-3000*.